Applied Mathematical Modelling 107 (2022) 332–352

Contents lists available at ScienceDirect

Applied Mathematical Modelling

journal homepage: www.elsevier.com/locate/apm

A robust unsupervised neural network framework for geometrically nonlinear analysis of inelastic truss structures

Hau T. Mai[a,b], Qui X. Lieu[c,d], Joowon Kang[e], Jaehong Lee[a,*]

[a] Deep Learning Architectural Research Center, Sejong University, 209 Neungdong-ro, Gwangjin-gu, Seoul 05006, Republic of Korea
[b] Faculty of Mechanical Engineering, Industrial University of Ho Chi Minh City, 12 Nguyen Van Bao Street, Ward 4, Go Vap District, Ho Chi Minh City 70000, Vietnam
[c] Faculty of Civil Engineering, Ho Chi Minh City University of Technology (HCMUT), 268 Ly Thuong Kiet Street, Ward 14, District 10, Ho Chi Minh City, Vietnam
[d] Vietnam National University Ho Chi Minh City (VNU-HCM), Linh Trung Ward, Thu Duc District, Ho Chi Minh City, Vietnam
[e] School of Architecture, Yeungnam University, 280, Daehak-Ro, Gyeongsan, Gyeongbuk 38541, Republic of Korea

ARTICLE INFO

Article history:
Received 24 September 2021
Revised 22 February 2022
Accepted 28 February 2022
Available online 9 March 2022

Keywords:
Neural networks
Geometrical and material nonlinearities
Loss function
Potential energy
Optimization
Truss

ABSTRACT

In this study, a robust and simple unsupervised neural network (NN) framework is proposed to perform the geometrically nonlinear analysis of inelastic truss structures. The core idea is to employ the NN to directly estimate nonlinear structural responses without utilizing any time-consuming incremental-iterative algorithms as those done in standard finite element method (FEM). To achieve such an objective, the loss function built via the total potential energy principle under boundary conditions (BCs) is minimized in the suggested NN model whose weights and biases are considered as design variables. In our computational framework, spatial coordinates of truss nodes are treated as input data, whilst corresponding displacement degrees of freedom are taken account of output. At the beginning of each training step, feedforward is performed to get the predicted displacement field, and it is used to derive the loss function based on the physical law. Then, back-propagation is applied to update the parameters of the network. This adjustment, which is the so-called learning process, is repeated until the potential energy is minimized. Once the network is properly trained, the mechanical responses of inelastic structures can be easily obtained. The suggested methodology is also extremely simple to implement, while the unlabeled data is available, small in size, independent of sampling techniques, and without finite element analyses (FEAs). Several benchmark examples regarding geometrical and material nonlinear analysis of truss structures are tested to show the effectiveness and reliability of the proposed paradigm. Obtained outcomes indicate that the developed NN framework is robust and can be extended to apply for other structures.

* Corresponding author.
E-mail addresses: maitienhaunx@gmail.com, maitienhau@iuh.edu.vn (H.T. Mai), lieuxuanqui@hcmut.edu.vn (Q.X. Lieu), kangj@ynu.ac.kr (J. Kang), jhlee@sejong.ac.kr (J. Lee).

https://doi.org/10.1016/j.apm.2022.02.036
0307-904X/

1. Introduction

Most mechanical behavior of structures is nonlinear in one way or another [1,2]. Due to the nonlinear changes of geometrical and material properties, designing structures under such responses becomes more complex and is required in analysis to obtain more accurate behavior [3,4]. A variety of algorithms for solving nonlinear structural problems have been proposed during the last few decades, and they are generally classified into two groups [5]. In the first one, the stiffness-based approach derived from the FEM employs incremental-iterative procedures such as incremental load method (ILM), Newton–Raphson, Quasi–Newton, Arc-length techniques, and so on, to update the stiffness matrix concerning the changes in the stress-strain relation and geometry of the structure. Owing to the salient advantanges of this methodology, it has been successfully applied in various nonlinear problems [6–12]. Nevertheless, the implementation of this approach still requires a large amount of numerical simulation works, depending on controlling parameters of the nonlinear incremental-iterative techniques. To circumvent this bottleneck, an alternative approach based on the minimum energy principle in combination with optimization schemes was developed to allow the direct determination of nonlinear responses without the requirement of any incremental-iterative strategies as those implemented in FEM [13]. According that core idea, several metaheuristic algorithms known as gradient-free methods have been successfully applied for the above issue, such as genetic algorithm (GA) [14], harmony search (HS) [15], and particle swarm optimization (PSO) [16] etc. Although these algorithms have the ability to search a near global optimum solution, they often require a larger number of evaluation functions and are of a relatively slow convergence speed. Besides, the gradient-based optimization algorithms have also been successfully applied in this context. For instance, Ohkubo et al. [17] developed a modified sequential quadratic programming algorithm for the structural analysis by solving potential energy minimization problem (PEMP) or complementary energy minimization problem (CEMP). In addition, an adaptive local search method (ALSM) was also released by Toklu [18]. Despite the fact that their convergence speed is fairly high, these methods always demand the compulsory calculation of derivative information of the energy function with respect to the displacements. This performance is one of the main difficulties in solving the problem, even imposible in many cases. Therefore, the NN with the ability to approximate any nonlinear function and its automatic differentiation has emerged as an efficient alternative tool to tackle this task.

In recent years, machine learning (ML) has attained remarkable success in many fields to help decision-making, e.g. speed recognition, industrial automation, medical diagnoses, material informatics, etc. Among ML models, NNs have attracted attention in computational mechanics such as structural analysis [19–21], materials sciences [22,23], fluid mechanics [24,25], structural optimization [26–29], structural healthy monitoring [30–34], fracture mechanics [35,36], and so on. As indicated by Li et al. [37], NN-based approaches can be categorized as purely data-driven and physics-informed ones. Accordingly, the data-driven methodology is often used to build surrogate models, while the other is employed to construct approximation spaces. The main difference between them is the training data which contains both input and expected output data for data-driven approach while the other only requires input data. More concretely, in structural analysis applications, the output data are the structural responses including displacement, stress, strain, and so on, whose values are often obtained through numerical methods in FEAs. In recent times, the data-driven approach has been successfully applied to solve complex structural analysis problems including linear [37–41] and nonlinear [42–47]. But they depend strongly on the numerical simulation results as well as size data [37,48]. Hence, it has not been an appropriate numerical tool for the structural analysis, especially for nonlinear problems. On the contrary, to overcome these difficulties, the physics-informed ML model is developed based on the governing physical laws which are integrated into the unsupervised learning process. It is worth mentioning that its training data only demands input data, and it contains the known output information about the problem. Indeed, this is one of the major strengths of this approach owing to the fact that it allows to establish an efficient NN-based computational framework without utilizing any conventional numerical simulations such as FEA. With this regard, there are two common approaches concerning the choice of loss function based on the energy and residual of partial differential equations (PDEs). And they have been successfully applied in several recent studies on structural analysis and fluid mechanics [49–54]. But this paradigm also depends significantly on the resolution of samples, sampling techniques, as well as the way of estimating a suitable training data size [37]. Furthermore, it has still not been yet utilized for geometrically nonlinear analysis of inelastic truss structures thus far.

Based upon the above-discussed investigations, this study aims at proposing an unsupervised NN model for geometrically nonlinear analysis of inelastic truss structures. Unlike other frameworks in the available literature, the training data of the proposed model is a set of the spatial coordinates of all joints which are easily collected from the connectivity information of the structure without any specific sampling techniques, as well as its small size. The training process aims to find the displacement field such that the total potential energy (TPE) is minimized. To do this, the feedforward (FF) as well as BCs are employed and applied to attain the predicted displacement field. Relied on these predictions and physical laws, the TPE is built as a loss function, and its gradients concerning parameters are computed by back-propagation (BP) to adjust weights and biases of the network. This process is repeated until the obtained minimum energy. Once the network is trained, it not only obtains the NN's optimal parameters but also identifies the nonlinear structural responses as soon as the training process ends without utilizing any incremental - iterative algorithms or FEAs. The efficiency and reliability of the presented approach are also investigated through several numerical examples.

The rest of this work is organized as follows. Section 2 provides the theoretical formulation of the TPE of truss structures. Next, a novel unsupervised NN-based approach is suggested in Section 3. In Section 4, several numerical examples are

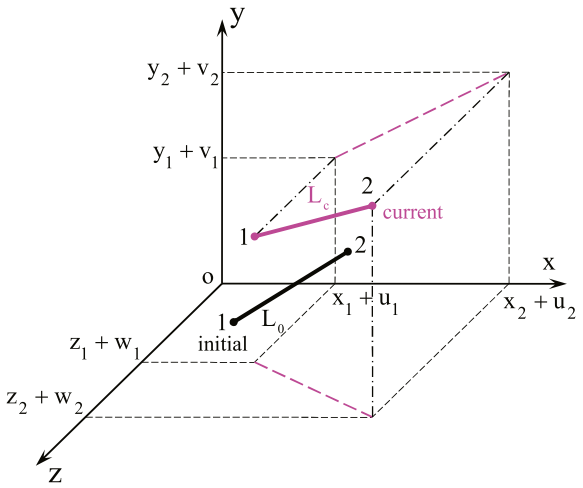

Fig. 1. Deformation of a space truss element.

investigated to demonstrate the efficiency and robustness of the presented method. Finally, crucial conclusions are outlined in Section 5.

2. Theoretical formulation

Structural analysis aims to obtain the responses for the equilibrium configuration under the action of external loads. In this section, the analysis of truss structures including linear and nonlinear behavior is described by minimizing the TPE [10,55]. Let us consider a truss-like structure that consists of n truss members and m nodes. Then the TPE of the system Π_p including the strain energy U and external work W can be expressed as [55]

$$\Pi_p = U + W, \tag{1}$$

in which

$$U = \sum_{k=1}^{n} e_k A_k L_k, \tag{2}$$

$$W = -\mathbf{P}^T \mathbf{u}, \tag{3}$$

$$e_k = \int_0^{\varepsilon_k} \sigma_k(\varepsilon_k) d\varepsilon_k, \tag{4}$$

where e_k, L_k, and A_k are the strain energy density, length, and cross-sectional area of the kth member; $\mathbf{u}$ is the vector of displacements at nodes; $\mathbf{P}$ denotes the vector of external forces; ε_k and σ_k are strain and stress of the kth member, and $\sigma(\varepsilon)$ expresses the stress-strain relation for the material of member.

In order to achieve the strain field, a space truss element with its initial configuration L_0 and current one L_c is considered as shown in Fig. 1. It is easily to compute L_0 and L_c of the element via coordinates of nodes $\left(x_i,\ y_i,\ z_i,\ x_j,\ y_j,\ z_j\right)$ and displacement field $\left(u_i,\ v_i,\ w_i,\ u_j,\ v_j,\ w_j\right)$. For more details, interested readers are suggested to consult Ref. [55,56].

Here, two frequently used strain models including engineering and Green strains for large displacement and small strain analysis are adopted in this work [56]. It should be noted that the stress-strain curve $\sigma(\varepsilon)$ can be linear, piecewise linear curve, or nonlinear, which depends on material properties and is assumed to be completely known for a given material type. Hence, if the displacements of member ends are determined, the strain and strain energy density of each member can be easily estimated by the integral Eq. (4).

According to the principle of minimum potential energy, the nodal displacements vector $\mathbf{u}$ are considered as unknown solutions and are determined by minimizing the TPE with BCs. Once the displacement field is found, the other structural responses can be completely determined by the constitutive equations.

3. Unsupervised learning-based approach framework

In this section, an unsupervised learning-based framework is developed to resolve the nonlinear analysis of truss structures. A flowchart of the overall proposed algorithm is illustrated in Fig. 2 where the parameters $\boldsymbol{\theta}$ including weights and biases of the network are design variables. According to this scheme, the network is set first up with the initial weight

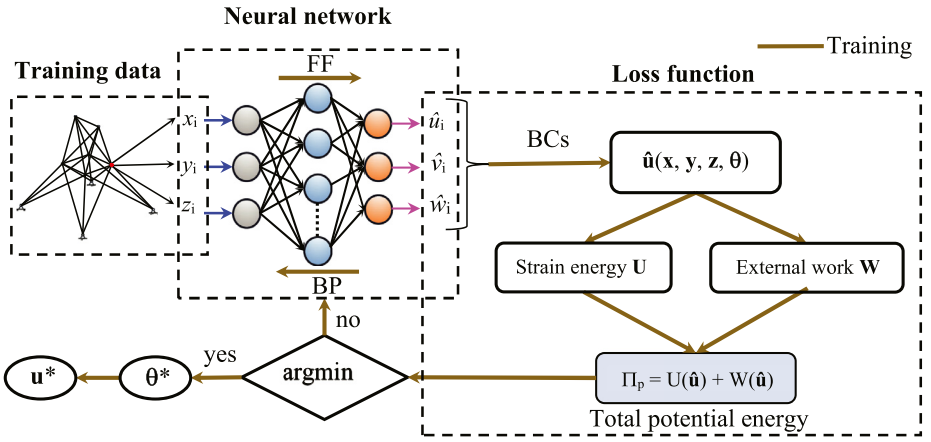

Fig. 2. The whole process of an unsupervised learning-based framework for geometrically nonlinear analysis of inelastic truss structures.

and bias values according to the normal distribution criterion. The coordinates of all nodes in the structure are used as the input training data, while the corresponding displacements are defined as the outputs obtained by the FF process. Based on these outputs, loads, BCs, and physical laws, the TPE including the strain energy and external force is established as the loss function which is minimized by adjusting weights and biases of the network. To achieve this goal, BP is employed to automatically calculate the sensitivity of the loss function with respect to the parameters, whereby they will be updated. The above computation is iterated and repeated many times, and it is called the learning process. Once the network is properly trained, the results in the context of nonlinear structural analysis can be found with minimum energy. In general, the presented approach consists of three main components, namely training data, NN, and loss function. They are represented in greater detail in the following sub-sections.

3.1. Training data

In contrast to most of the previous approaches which utilized supervised learning models [42,57,58], the framework presented here relies on unsupervised learning. The main distinction between them is that the output data is not given in unsupervised learning. In other words, the responses of the structure including displacement, strain, stress, member force, etc. are not included in the training data. It means that we only have input data including a set of coordinates (x_i, y_i, z_i) of all structural nodes for the learning process. Hence, the training data is easily obtained from the geometry of the structure and completely independent of sampling techniques. Additionally, its size is small $(m \times 2)$ and $(m \times 3)$ for planar and space truss structures, respectively. Here m denotes the number of nodes, while 2 or 3 implies the number of spatial coordinates for 2- or 3-dimensional truss.

3.2. Neural network

NN is one of the machine learning models used to represent a set of mathematical relationships between the inputs and outputs through a training process as the working way of the human brain. For illustration, a fully connected NN with 3 layers is depicted in Fig. 3. Therein, the input layer is known as the first layer which consists of three neurons corresponding with the spatial coordinates (x, y, z), the second layer as hidden layer consists of m_h neurons which depends on the complexity of the application, and the last layer is called the output layer with three neurons which corresponds to the predicted displacements $(\hat{u}, \hat{v}, \hat{w})$. And the neurons of the present layer are connected to all units in the previous layer via the parameters of the NN which consists of weights $\mathbf{W}^{(l)}$ and biases $\mathbf{b}^{(l)}$, respectively.

To train the network, both FF and BP processes are employed to adjust the parameters of the NN and are repeated over and over until the loss converges to a minimum value. Specifically, in the FF process, a mapping from input to output nodes can be expressed as $\hat{\mathbf{I}}$: $\mathbb{R}^3 \to \mathbb{R}^3$. The data is transmitted from the first layer to the last layer by the transformations. Hence, the relation between the input and output of each layer is expressed as

$$\begin{aligned} \text{input layer} \quad &: \quad \hat{\mathbf{o}}^0 = [x, y, z] \in \mathbb{R}^3, \\ \text{hidden layer:} \quad &\hat{\mathbf{o}}^1 = f_1\left(\mathbf{W}^1\hat{\mathbf{o}}^0 + \mathbf{b}^1\right) \in \mathbb{R}^{m_h}, \\ \text{output layer} \; : \quad &\hat{\mathbf{o}}^2 = f_2\left(\mathbf{W}^2\hat{\mathbf{o}}^1 + \mathbf{b}^2\right) = \left[\hat{u}, \hat{v}, \hat{w}\right] \in \mathbb{R}^3, \end{aligned} \tag{5}$$

where $f_1(.)$ and $f_2(.)$ are in turn the activation function for hidden and output layers, which supports the network to learn the nonlinear relationship between input and output, and make accurate predictions. Several common choices include Linear, ReLU, LeakyReLU, Sigmoid, Softmax, and Tanh. $\hat{\mathbf{o}}^1$ and $\hat{\mathbf{o}}^2$ denote the output of the hidden and output layers, respectively.

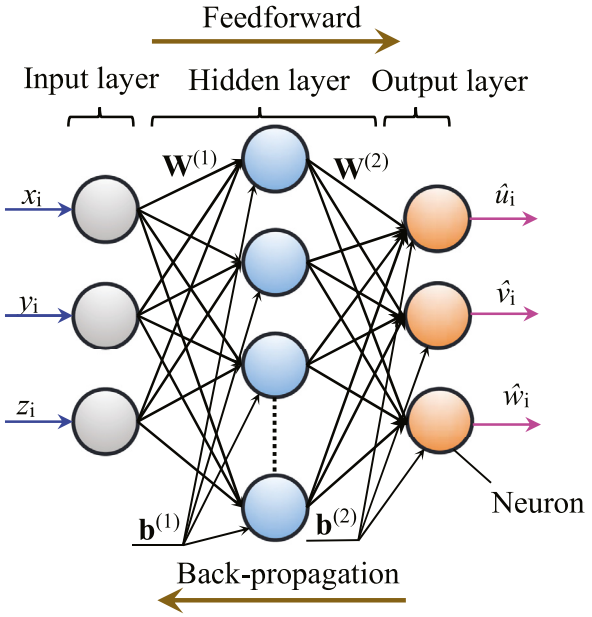

Fig. 3. Architecture of a fully-connected multi-layer network.

To identify optimal parameters, an optimization process, which is the so-called network training, is performed to minimize the loss function $\mathcal{L}$. To do this, BP is required to obtain the gradient information of the loss with respect to the weights and biases. And then, they are updated in the direction of the gradient descent, as expressed below

$$
\begin{aligned}
{}^{t+1}W^l_{pq} &= {}^{t}W^l_{pq} - \eta \frac{\partial \mathcal{L}}{\partial {}^{t}W^l_{pq}}, \\
{}^{t+1}b^l_{p} &= {}^{t}b^l_{p} - \eta \frac{\partial \mathcal{L}}{\partial {}^{t}b^l_{p}} \qquad for\ \ 1 \le l \le 2,
\end{aligned} \tag{6}
$$

where η is the learning rate; p and q are the number of neurons in the lth and $(l-1)$th layer, respectively; t denotes the iteration index. Finally, the parameters will converge to the minimum loss value after an iterative process.

3.3. Loss function

As mentioned above, the outputs of the NN are the displacements expressed by the parameters including weights and biases of the network. Then, the TPE is computed by a sum of the strain energy and external work based on the outputs, loads, and BCs. And this term serves as a loss function which is minimized in the training process. Its mathematical expression is given as follows

$$
\mathcal{L}(\boldsymbol{\theta}) = U\left(\hat{\mathbf{u}}(\boldsymbol{\theta})\right) + W\left(\hat{\mathbf{u}}(\boldsymbol{\theta})\right), \tag{7}
$$

where $\hat{\mathbf{u}}$ is the predicted displacement vector; $\boldsymbol{\theta}$ is the parameter vector including weights and biases of the network.

It should be noted that the loss function only contains the predicted displacements and this is an advantage of algorithm based on unsupervised learning. At the same time, it is easily seen that instead of solving the nonlinear analysis problem by using incremental-iterative methods, we now turn to minimize the loss function by training to find the optimal parameters $\boldsymbol{\theta}^*$ of the NN.

$$
\boldsymbol{\theta}^* = \arg\min_{\boldsymbol{\theta}} \left(\mathcal{L}(\boldsymbol{\theta}) \right). \tag{8}
$$

It is also worth mentioning that the sensitivity of the loss function to parameters can be easily and automatically calculated by using NN's back-propagation. In this work, the training of the network is terminated when either the maximum number of epoch reaches or the norm of the gradient value is less than a threshold value of 0.01 [59]. Once the network is trained, the displacement field and corresponding structural responses can be found.

4. Numerical experiments

In this section, several numerical examples are explored to demonstrate the efficiency of the proposed approach for nonlinear analysis of truss structures including geometric nonlinearity, material nonlinearity, and dual nonlinearities. For that

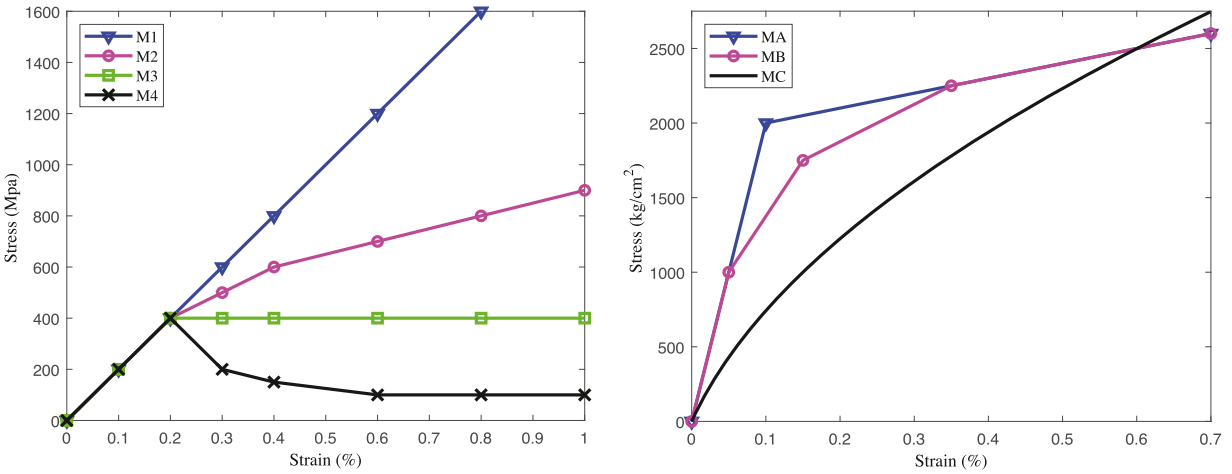

Fig. 4. Stress - strain relationships considered in the analysis.

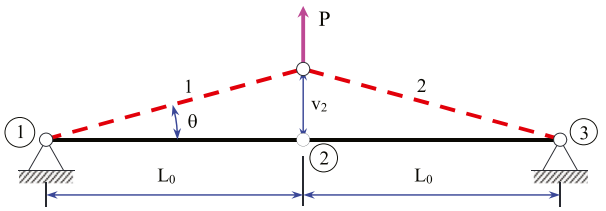

Fig. 5. Schematic of a two-bar planar truss.

purpose, the obtained results from the presented work are compared with those of other studies available in the literature. In all considered examples, the number of units in the input and output layers is equal to 2 or 3 for 2D or 3D problems, respectively. Meanwhile, Grid search and trial error methods are used to determine the number of neurons in the hidden layers. For training, an Adam optimizer is employed to update the parameters of the network with the learning rate 0.01 [60]. Tanh and Linear are the activation functions chosen for the hidden and output layers, respectively. All experiments are implemented on a desktop computer with Core i5-8500 CPU of @3.0 GHz and 16 GB RAM.

4.1. Material and geometrical nonlinearities

In this part, seven different types of materials are considered for geometrically nonlinear analysis of inelastic truss structures with the stress - strain relationships, as depicted in Fig. 4. In which, the first group includes four type of materials which are denoted from MAT1 to MAT4 and built based on piecewise linear curves M1–M4 as shown on Fig. 4a. Therein, the strain-stress relation of MAT4 is unsymmetrical with respect to M4 in compression and M3 in tension while the others are symmetrical. In the second group, three types of materials MATA, MATB, and MATC are the symmetrical stress-strain relations in tension and compression, and obtained from piecewise linear curves of MA, MB, and MC, as depicted in Fig. 4b. It should be noted that the relation given for MATC is defined by $\varepsilon = 6 \times 10^{-10}\sigma^2 + 9 \times 10^{-7}\sigma$.

4.1.1. Two-bar truss

A two-bar truss subjected to a vertical load P = 100 N at the middle point is investigated as the first example for the nonlinear analysis, as depicted in Fig. 5. The cross-sectional area and length of all members are set as $A = 1$ mm^2 and $L_0 = 1000$ mm, respectively. Two types of materials, namely MAT1 and MAT3, are considered to evaluate the effects of only geometric nonlinearity and both material and geometric nonlinearities. According to Ref. [18], the analytical solution for geometrical nonlinearity is given as follows

$$\begin{cases} v_2 = L_0 \tan(\theta), \\ f_1 = f_2 = \frac{P}{2\sin(\theta)}, \\ \tan(\theta)(1 - \cos(\theta)) = \frac{P}{2AE}. \end{cases} \tag{9}$$

Firstly, several different combinations of activation functions and optimizers are adopted to identify the best combination under the same network architecture (2-10-2) with linear activation function in the output layer for material MAT1. The relative errors of the exact and the predicted potential energies are reported in Table 2. It can be seen from the data in this

Table 1
Type of material, number of hidden neurons, and epoch for different problems.

Problem	Material type	Network architecture	Epoch
2-bar truss	MAT1, 3	(2-10-2)	500
6-bar truss	MAT1, 2	(2-10-2)	500
	MAT3, 4	(2-100-2)	1000
31-bars truss	MATA, B, C	(2-50-2)	2000
25-bar truss	MAT5	(3-50-3)	1000
52-bar truss	MAT6	(3-50-3)	1000
10-bar truss	MATA, B, C	(2-10-2)	500
21-bar truss	MATA, B, C	(2-10-2)	500

Table 2
Relative error of minimum TPE (10^{-5}) with various optimizers and activation functions.

Activation function	Optimizers					
	Adam	RMSprop	Adadelta	SGD	Adagrad	Adamax
Softmax	1.8094	33.3622	476.3840	617.8942	6451.9175	3.3428
Softplus	0.0449	73.9318	52.2400	1.5435	24.8778	0.1206
Tanh	**0.0022**	9.1730	5.6941	0.2552	12.1375	0.0672
Sigmoid	0.0389	10.0903	979.9133	0.1384	24.6756	0.1938
ReLU	0.0819	17.2319	250.2252	3.2209	34.0667	0.5480

Table 3
Relative error of deflection (10^{-7}) with various neurons and hidden layers.

No. of hidden layers	No. of hidden neurons				
	10	20	30	40	50
1	**0.2236**	0.7362	0.7362	1.1833	31.8947
2	2.1430	0.7362	1.6959	22.3579	84.1400
3	2.6556	5.0222	5.0222	12.2529	28.0558
4	4.0625	3.6153	1.6959	20.8905	82.7604

Table 4
Effect of different strain models for geometrically nonlinear responses of two-bar truss.

Strain	v_2(mm)		$f_{1,2}$ (N)		Π_p(kN.mm)	
	Exact	Present	Exact	Present	Exact	Present
Engineering	79.4952	79.4952	630.9532	630.9531	−5.9590	−5.9590
Green	79.4952	79.3701	631.9484	629.9609	−5.9527	−5.9528
Log	79.4952	79.6213	629.9600	631.9538	−5.9653	−5.9653
Almansi	79.4952	79.8764	627.9799	633.9797	−5.9777	−5.9780

table that Adam is the best optimizer among all with the lowest relative errors. Meanwhile, Tanh is either the best or the second best in the combination of the other activation functions with optimizers. The result obtained by combining Tanh and Adam is of the smallest error (0.22×10^{-7}), so they are chosen for the implementation in this work. Additionally, the impact of varying neurons and hidden layers in the network is also investigated to assess the predicted accuracy. According to the errors attained from Table 3, increasing the number of neurons and hidden layers can not improve the performance of the model, and the NN architecture (2-10-2) shown in Table 1 is the best selection to solve this example.

Next, various strain models are considered to estimate their effect on the geometric nonlinear analysis. As shown in Table 4, it is easily seen that the results achieved by the NN agree well with the analytical values for all strain models, while the engineering strain is the best model with the small relative errors (1.58×10^{-7}). Thus, it is utilized throughout the present work.

As can be seen from Table 5, the analysis results obtained from the NN, including deflection (v_2), member forces ($f_{1,2}$), as well as minimum potential energy (Π_p) are a very good agreement with the analytical and ALSM outcomes. The convergence curve of the NN is illustrated in Fig. 6. It also indicates that the convergence speed accelerates in the early period of epoch and approaches the optimal energy after only 150 epochs for two types of materials. In addition to considering the effect of geometric and material nonlinearities on the structure, the variation of the external force is also investigated here. Corresponding to this change, the behavior of the system is shown in Fig. 7, where the energies and deflections are in keeping with previous observational studies. On the other hand, it can be seen that the material nonlinearity has a great influence on the structural responses when the load P is greater than 50.5207(N). Hence, the obtained analysis results point out that NN is reliable and stable for solving nonlinear problems.

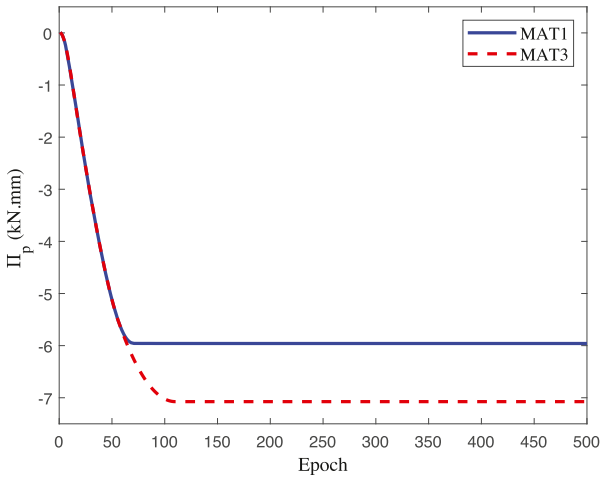

Fig. 6. The convergence histories of the loss function for the two-bar truss with the materials MAT1 and MAT3.

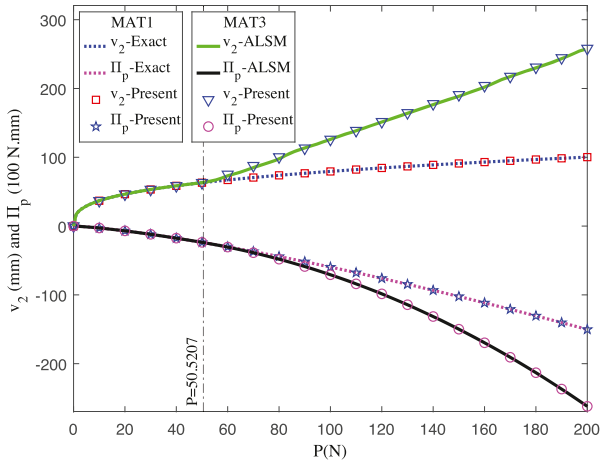

Fig. 7. Responses of the 2-bar truss structure with varying external force.

Table 5
Comparison of analysis results for two-bar truss with different materials.

	MAT1		MAT3	
	Exact	Present	ALSM [18]	Present
v_2(mm)	79.4952	79.4952	125.9875	125.9882
$f_{1.2}$ (N)	630.9532	630.9531	400.0000	400.0000
Π_p(kN.mm)	−5.9590	−5.9590	−7.0746	−7.0746

4.1.2. Six-bar truss

The next example analyzes a 6-bar planar truss structure with the geometry, finite element representation, loads, and boundary conditions as depicted in Fig. 8. Here, members 2–4 have the same cross-sectional area of 100 mm^2, while the remaining ones are 200 mm^2. In this example, material MAT1 is considered for both linear and geometric nonlinear analyses. Three material types MAT2 to MAT4 are valid for material and geometric nonlinearities. This benchmark problem was previously analyzed by Toklu [18] using ALSM. Table 1 lists the details of network architectures used to train the model.

As shown in Tables 6 and 7, the obtained solutions reveal that the presented method is highly close to those found in literature [18]. At the same time, it is easily be seen that the results of the linear and geometric nonlinear analysis are practically the same, so the influence of geometry changes is small for this loading. But the effect of the material and geometric nonlinearities is significant on the response of structure, where the horizontal displacement at node 4 increases 10, 138, and 159 times for MAT2, MAT3, and MAT4, respectively. Moreover, it is also worthwhile emphasizing that the member force of elements 1–4 reaches the yield point for MAT3 and MAT4 as the data in Table 7. Fig. 9 shows the TPE

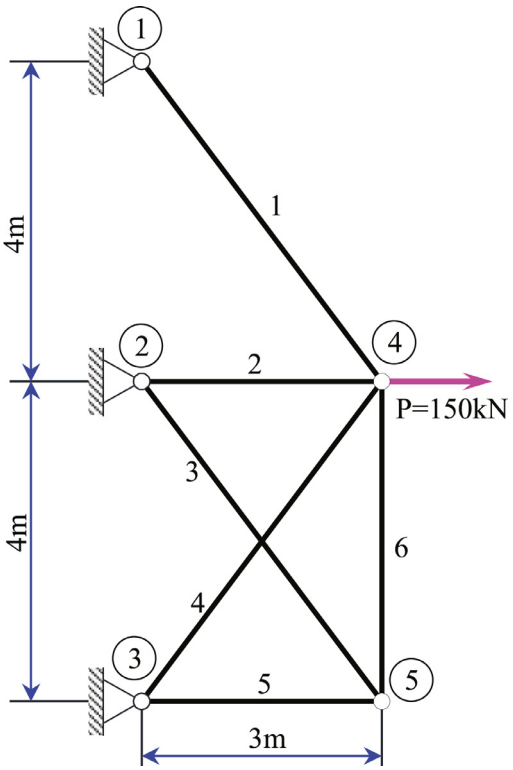

Fig. 8. A 6-bar planar truss structure.

Table 6
Comparison of joint displacements and energy for 6-bars truss with different solution techniques and different materials.

Disp no. (mm)	Linear		Nonlinear							
	MAT1		MAT1		MAT2		MAT3		MAT4	
	FEM	Present	ALSM [18]	Present	ALSM [18]	Present	ALSM [18]	Present	ALSM [18]	Present
u_4	14.1497	14.1508	14.12	14.1199	139.71	139.7093	1931.60	1931.5973	2235.51	2235.5098
v_4	2.8427	2.8431	2.83	2.8281	28.46	28.4541	−403.79	−403.7856	387.11	387.1073
u_5	0.3001	0.3059	0.30	0.3016	3.30	3.2974	1.89	1.8945	−283.55	−283.5538
v_5	2.3092	2.3104	2.32	2.3167	25.00	24.9958	88.17	88.1705	1277.18	1277.1859
Π_p(kN.m)	−1.061227	−1.061228	−1.059735	−1.059735	−11.27096	−11.27090	−36.75831	−36.75831	−52.09811	−52.09811

Table 7
Comparison of member forces for 6-bars truss with different solution techniques and different materials.

Forces (kN)	Linear		Nonlinear							
	MAT1		MAT1		MAT2		MAT3		MAT4	
	FEM	Present	ALSM [18]	Present	ALSM [18]	Present	ALSM [18]	Present	ALSM [18]	Present
f_1	49.7251	49.7220	49.811	49.8106	50.163	50.1616	80.000	80.0000	80.000	80.0000
f_2	94.3313	94.3279	94.142	94.1414	93.190	93.1913	40.000	40.0000	40.000	40.0000
f_3	−6.6691	−6.6699	−6.688	−6.6884	−7.195	−7.1948	−40.000	−40.0000	−10.000	−10.0000
f_4	43.0560	43.0551	42.974	42.9743	41.494	41.4934	40.000	40.0000	40.000	40.0000
f_5	4.0015	3.9993	4.035	4.0334	4.535	4.5352	42.512	42.5207	22.839	22.8460
f_6	5.3353	5.3353	5.352	5.3527	5.782	5.7816	37.642	37.6375	21.616	21.6090

convergence histories obtained using NN with the materials MAT3 and MAT4. One again shows that the convergence speed is high at initial epochs and quickly stabilizes after 250, and 500 epochs for the respective materials.

Fig. 10 shows the structural responses obtained from changing the external force between −200N and 200N. Note that when the applied load P is in the range from −120N to −50N, the deflection and energy decrease suddenly, and the member forces increase. It indicates that the proposed approach can predict the snap-though of structures.

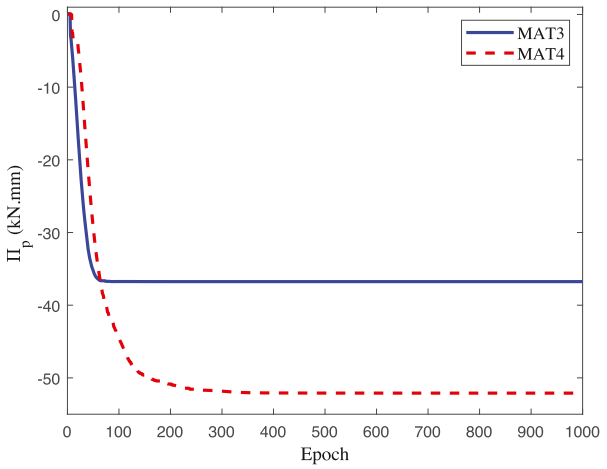

Fig. 9. The convergence histories of the loss function for the 6-bar truss with the materials MAT3 and MAT4.

Table 8
Comparision of joint displacement results for the 31-bars truss with different algorithms and various materials.

Disp no. (cm)	MATA				MATB				MATC		
	PEMP [17]	ILM [17]	ALSM [18]	Present	PEMP [17]	ILM [17]	ALSM [18]	Present	ILM [17]	ALSM [18]	Present
v_2	−49.0250	−49.4760	−49.5110	−49.5115	−50.2590	−50.7820	−50.7920	−50.7922	−35.9990	−49.5160	−35.9625
v_3	−87.3740	−87.5870	−87.3880	−87.3888	−89.5110	−89.5920	−89.5710	−89.5710	−63.4660	−87.3960	−63.4037
v_4	−94.1930	−94.2510	−94.0710	−94.0710	−95.8230	−95.7800	−95.7530	−95.7536	−66.2580	−94.0800	−66.1736
v_5	−73.8380	−74.0970	−74.0530	−74.0530	−75.0940	−75.3490	−75.3550	−75.3554	−52.9870	−74.0600	−52.9275
u_8	47.9770	48.5100	48.5390	48.5397	47.9750	48.5820	48.5830	48.5835	32.4500	48.5440	32.4115
v_9	−53.5500	−52.3870	−51.8250	−51.8259	−54.7240	−53.2240	−53.0710	−53.0708	−37.0310	−51.8300	−36.8826
v_{10}	−87.9930	−87.8630	−87.5170	−87.5176	−89.8660	−89.5490	−89.4520	−89.4522	−62.3390	−87.5250	−62.2022
v_{11}	−94.3830	−94.4190	−94.2040	−94.2042	−96.0290	−95.9450	−95.8990	−95.8988	−66.4220	−94.2130	−66.3187
v_{12}	−75.5780	−75.2380	−74.9540	−74.9539	−76.8780	−76.3420	−76.2790	−76.2791	−53.4150	−74.9610	−53.3082
Π_p(t.m)	–	–	−114.7	−114.7019	–	–	−119.3	−119.2682	–	−104.6	−107.6307

Table 9
Comparision of member forces for the 31-bars truss with different algorithms and various materials.

Forces (t)	MATA				MATB				MATC		
	PEMP [17]	ILM [17]	ALSM [18]	Present	PEMP [17]	ILM [17]	ALSM [18]	Present	ILM [17]	ALSM [18]	Present
f_2	442.80	444.60	443.11	443.0873	442.30	440.90	441.31	441.3054	430.00	443.11	428.9959
f_3	514.80	509.90	512.61	512.5867	512.50	507.10	510.63	510.6323	500.70	512.61	501.2984
f_4	397.60	397.00	397.82	397.7927	397.90	396.40	397.93	397.9342	397.20	397.82	397.3081
f_5	278.10	278.60	278.61	278.5943	278.30	278.50	278.76	278.7565	277.30	278.61	277.0117
f_8	−430.70	−432.50	−431.67	−431.6603	−430.70	−434.20	−433.19	−433.1843	−437.30	−431.67	−436.8997
f_9	−504.80	−511.60	−509.98	−509.9564	−506.90	−515.30	−511.94	−511.9359	−520.40	−509.98	−519.4853
f_{10}	−389.90	−392.10	−392.08	−392.0528	−389.70	−393.20	−392.09	−392.0928	−392.00	−392.08	−391.5264
f_{11}	−278.00	−278.30	−278.49	−278.4798	−277.90	−278.60	−278.47	−278.4709	−278.70	−278.49	−278.6257
f_{20}	−203.00	−202.60	−202.72	−202.7261	−203.30	−203.10	−203.32	−203.3112	−210.50	−202.72	−210.7070
f_{27}	204.70	207.40	206.15	206.1441	205.00	210.00	208.42	208.4275	215.00	206.15	214.5896

4.1.3. Thirty-one-bar truss

In the third example, the analysis problem of the 31-bar planar truss is investigated. This issue was previously addressed by Toklu [18] and Ohkubo [17]. The geometry, dimensions, loads, boundary conditions, and finite element representation are depicted in Fig. 11. The cross-sectional area of all members is 100 cm^2. Three types of materials including MATA, MATB, and MATC are considered for combining geometric and material nonlinearities. The network configuration, as shown in Table 1, is built to train the model.

As previously investigated examples, the analysis results gained by the presented work are reported in Tables 8 and 9 for comparison with other algorithms. It is easily seen that the minimum energy, displacements, and member forces obtained by NN show a strong agreement for both MATA and MATB materials. Meanwhile, for MATC material, the NN results are very close to ILM [17], and better than ALSM [18] when the optimal energy (−107.6307 t.m) is smaller than ALSM (−104.6 t.m). Note, however, that the optimal energies of three types of materials are similar together. It is easily explained that the stress-strain relationship curves of different materials are quite analogous. Fig. 12 displays the convergence curves of NN for

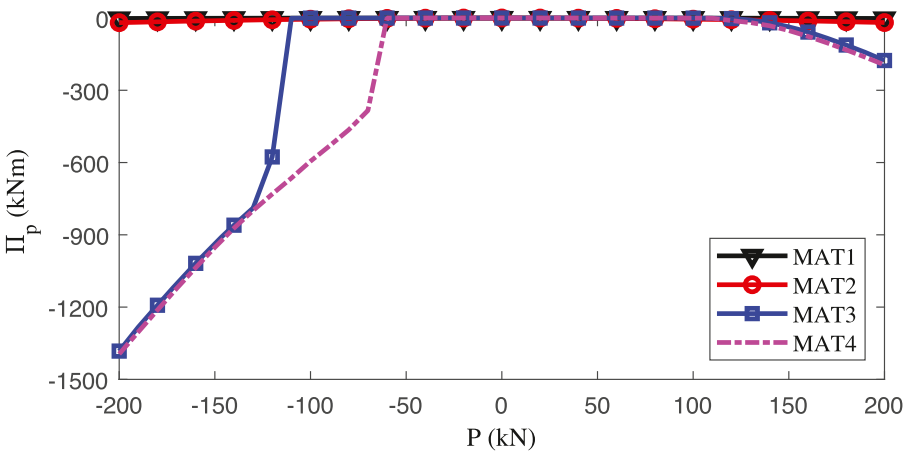

(a) Total potential energy

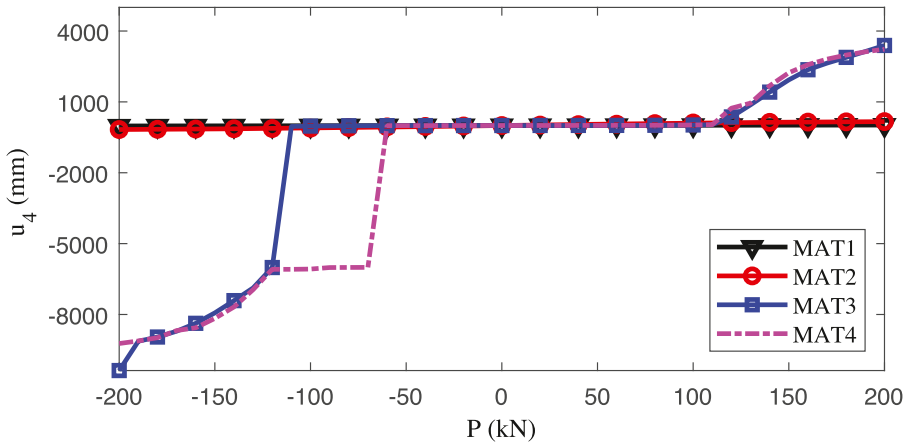

(b) Horizontal displacement of joint 4

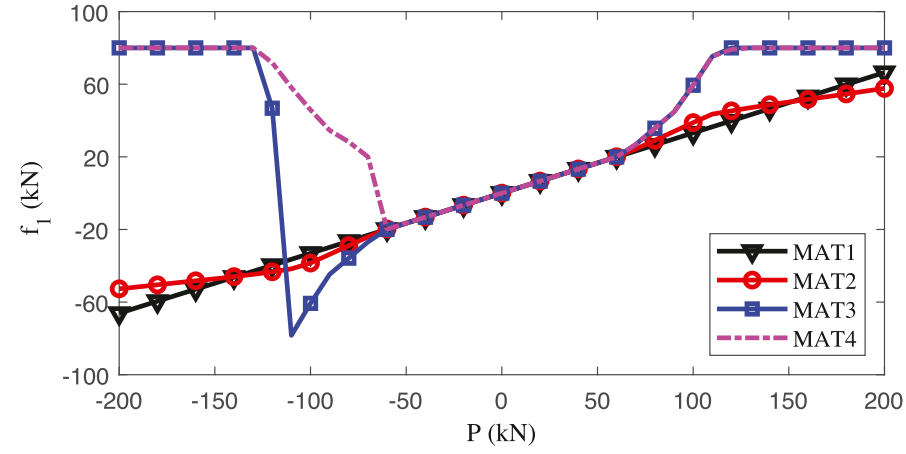

(c) Internal force of the member 1

Fig. 10. Potential energy, deflection, and the first member force with various external force levels for the 6-bar truss with different materials.

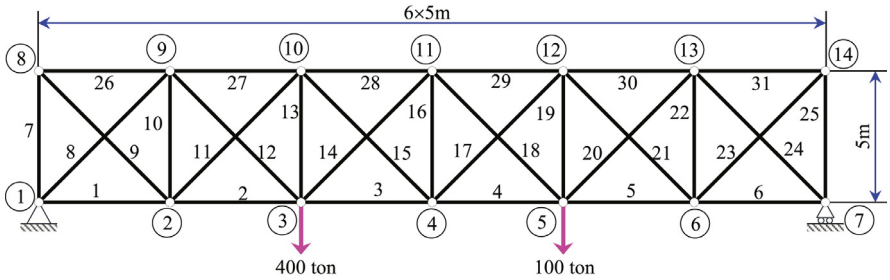

Fig. 11. A 31-bar planar truss structure.

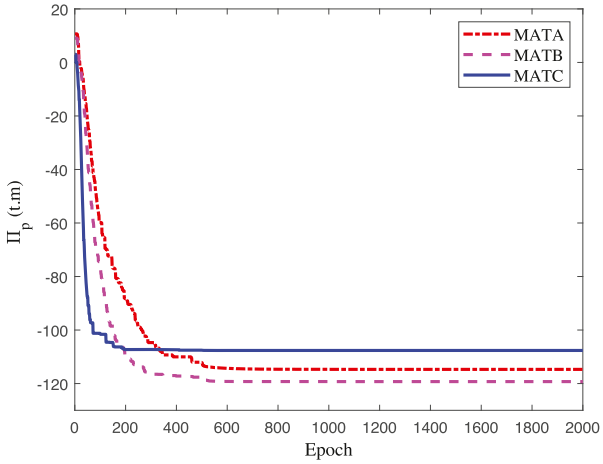

Fig. 12. The convergence histories of the loss function for the 31-bar truss with different materials.

Table 10
Loading conditions for the 25-bar space truss with geometrical nonlinearity.

Node	Case 1 (kN)			Case 2 (kN)			Case 3 (kN)		
	F_x	F_y	F_z	F_x	F_y	F_z	F_x	F_y	F_z
1	0	80	−20	800	0	−200	800	800	−200
2	0	−80	−20	−800	0	−200	0	0	0

different materials. From this graph, we can see that MATC and MATB create the most rigid and flexible structure under this loading, respectively.

4.2. Geometrical nonlinearity

4.2.1. 25-bar space truss

Next, a space truss with 25 members illustrated in Fig. 13 is investigated for the geometrically nonlinear analysis. All members are assigned to MAT5 with the same linear elastic modulus 2×10^5 N/mm^2 and the same cross-sectional area 10 mm^2. Three loading cases given in Table 10 are considered. In addition, a NN (3-50-3) is constructed for the training stage with 1000 epochs.

A comparison of the analysis results obtained by the present study and other methods [16] are reported in Tables 11 and 12. From the data in these tables, the gained results are quite close to each other in all loading cases. However, the differences between HS, PSO, and this work are represented by the relative error with respect to the FEM solution, as shown in Table 13. More specifically, the maximum error of the NN is bounded and less than 0.5%, while HS and PSO gained up to 6.5777% and 5.3105%, respectively. Furthermore, the average error of the present method is the smallest and less than 0.05%. On the other hand, it only requires 1000 evaluations to converge for all loading cases, while HS [15] takes 100,000 for all cases and PSO [16] takes 1000, 20,000, and 50,000 for each case, respectively. The above experimental results have revealed that the present approach can significantly improve the convergence rate compared with other methods but still ensuring the quality of solution.

Table 11
Comparison of displacements for 25-bars truss with various loading conditions.

Disp no. (mm)	Case 1				Case 2				Case 3			
	HS [15]	PSO [16]	FEM [16]	Present	HS [15]	PSO [16]	FEM [16]	Present	HS [15]	PSO [16]	FEM [16]	Present
u_1	−0.076	0.06	0.000	0.0000	1257.533	1260.63	1261.101	1261.0713	2522.412	2521.86	2522.974	2522.9897
v_1	37.910	38.01	37.847	37.8463	−527.509	−529.80	−528.823	−528.6810	1840.283	1839.88	1840.856	1840.8893
w_1	−37.214	−37.27	−37.199	−37.1997	−455.548	−455.35	−456.667	−456.7458	−3078.900	−3076.40	−3083.146	−3083.3000
u_2	−0.064	0.06	0.000	0.0000	−1264.620	−1261.15	−1261.101	−1261.1061	2437.300	2435.57	2441.255	2441.4587
v_2	−37.766	−37.68	−37.847	−37.8472	529.739	529.20	528.823	528.6903	2522.971	2522.31	2523.148	2523.1187
w_2	−37.153	−37.16	−37.199	−37.1991	−457.905	−455.38	−456.667	−456.7199	−1435.857	−1433.56	−1441.611	−1441.8916
u_3	0.892	0.86	0.867	0.8669	−48.858	−47.50	−48.610	−48.7118	−393.940	−393.83	−394.610	−394.6388
v_3	−1.731	−1.73	−1.744	−1.7441	−288.344	−287.03	−288.313	−288.4180	−371.211	−371.22	−371.344	−371.3444
w_3	−16.342	−16.45	−16.392	−16.3924	−362.120	−361.33	−362.743	−362.8435	−904.675	−903.69	−905.218	−905.2232
u_4	0.924	0.88	0.867	0.8668	−203.107	−203.19	−202.750	−202.7069	579.074	579.02	579.039	578.9871
v_4	1.750	1.76	1.744	1.7444	−296.619	−295.57	−296.792	−296.8928	198.927	198.35	199.088	199.0949
w_4	−16.355	−16.38	−16.392	−16.3914	−67.535	−68.84	−68.466	−68.4153	44.972	45.45	44.423	44.4499
u_5	−0.822	−0.85	−0.867	−0.8669	48.774	47.10	48.610	48.7141	1013.812	1012.54	1015.303	1015.3925
v_5	1.751	1.78	1.744	1.7444	288.714	286.57	288.313	288.4188	1037.329	1036.29	1038.580	1038.6544
w_5	−16.402	−16.35	−16.392	−16.3913	−363.583	−361.26	−362.743	−362.8326	−353.069	−351.08	−356.179	−356.4052
u_6	−0.844	−0.87	−0.867	−0.8669	202.232	202.95	202.750	202.7087	407.347	406.51	408.348	408.3932
v_6	−1.746	−1.70	−1.744	−1.7443	297.259	295.18	296.792	296.8958	802.637	802.21	803.160	803.1612
w_6	−16.430	−16.40	−16.392	−16.3922	−69.186	−68.67	−68.466	−68.4220	−36.622	−36.68	−36.688	−36.6542
Π_p(kN.m)	−3.7645	−3.7645	−3.7645	−3.7645	−1444.60	−1444.60	−1444.60	−1444.59	−2860.50	−2860.50	−2860.50	−2860.49

Table 12
Comparison of member forces for 25-bars truss with various loading conditions.

Forces (kN)	Case 1				Case 2				Case 3			
	HS [15]	PSO [16]	FEM [16]	Present	HS [15]	PSO [16]	FEM [16]	Present	HS [15]	PSO [16]	FEM [16]	Present
f_1	75.676	75.690	75.693	75.6935	692.590	691.627	692.496	692.5688	107.640	107.691	106.578	106.5109
f_2	3.915	3.902	3.893	3.8928	−334.408	−334.677	−334.607	−334.5806	273.603	273.432	274.288	274.3303
f_3	3.883	3.869	3.893	3.8940	73.046	73.231	72.764	72.7525	−310.372	−310.660	−310.686	−310.7146
f_4	3.890	3.898	3.893	3.8927	72.343	73.245	72.764	72.7250	247.023	247.501	246.394	246.3438
f_5	3.885	3.881	3.893	3.8938	−334.711	−334.761	−334.607	−334.5647	−70.532	−70.574	−70.015	−69.9877
f_6	−13.844	−13.879	−13.883	−13.8831	275.294	275.049	274.675	274.6401	−10.172	−10.110	−10.677	−10.7257
f_7	−13.875	−13.874	−13.883	−13.8832	−189.137	−189.519	−189.233	−189.2128	359.301	359.219	359.449	359.4599
f_8	−13.899	−13.909	−13.883	−13.8829	−189.279	−189.291	−189.233	−189.2280	187.014	186.599	187.700	187.7289
f_9	−13.894	−13.907	−13.883	−13.8830	273.927	275.003	274.676	274.6107	471.844	471.760	472.059	472.0688
f_{10}	1.736	1.730	1.734	1.7338	−132.535	−132.998	−132.732	−132.7007	−110.993	−111.052	−111.426	−111.4535
f_{11}	1.745	1.730	1.734	1.7337	−132.868	−132.948	−132.732	−132.7026	−180.275	−179.696	−180.523	−180.5569
f_{12}	−3.482	−3.490	−3.489	−3.4885	35.618	35.618	35.767	35.7734	−26.908	−26.821	−26.811	−26.8122
f_{13}	−3.497	−3.480	−3.489	−3.4887	35.798	35.781	35.767	35.7730	−106.789	−106.819	−106.798	−106.8088
f_{14}	−3.376	−3.413	−3.489	−3.4851	−52.294	−51.883	−52.346	−52.3840	−260.641	−260.427	−260.940	−260.9510
f_{15}	−3.412	−3.402	−3.489	−3.4851	−125.339	−125.189	−125.277	−125.2644	−237.250	−236.904	−237.647	−237.6528
f_{16}	−3.366	−3.385	−3.489	−3.4849	−125.143	−125.368	−125.277	−125.2618	238.850	238.851	238.741	238.7296
f_{17}	−3.412	−3.385	−3.489	−3.4848	−52.509	−51.825	−52.346	−52.3824	−177.597	−177.046	−178.359	−178.4138
f_{18}	−4.657	−4.660	−4.656	−4.6558	116.226	115.587	116.025	116.0641	−125.783	−125.457	−125.978	−125.9688
f_{19}	−4.643	−4.664	−4.656	−4.6560	−174.651	−174.273	−174.822	−174.8633	−248.091	−247.944	−248.093	−248.0878
f_{20}	−4.654	−4.656	−4.656	−4.6558	−174.651	−174.273	−174.822	−174.8608	−190.078	−189.732	−190.717	−190.7642
f_{21}	−4.662	−4.643	−4.656	−4.6560	115.946	115.450	116.025	116.0639	332.335	332.074	332.665	332.6797
f_{22}	−7.378	−7.385	−7.367	−7.3677	−46.776	−45.834	−46.168	−46.1846	−52.549	−52.744	−52.285	−52.2527
f_{23}	−7.355	−7.397	−7.367	−7.3678	−54.925	−55.429	−55.264	−55.2386	−106.707	−106.436	−106.579	−106.5696
f_{24}	−7.365	−7.361	−7.367	−7.3672	−45.581	−45.918	−46.168	−46.1814	−50.752	−50.697	−50.960	−50.9357
f_{25}	−7.358	−7.333	−7.367	−7.3672	−55.421	−55.700	−55.264	−55.2332	542.045	541.876	542.082	542.0712

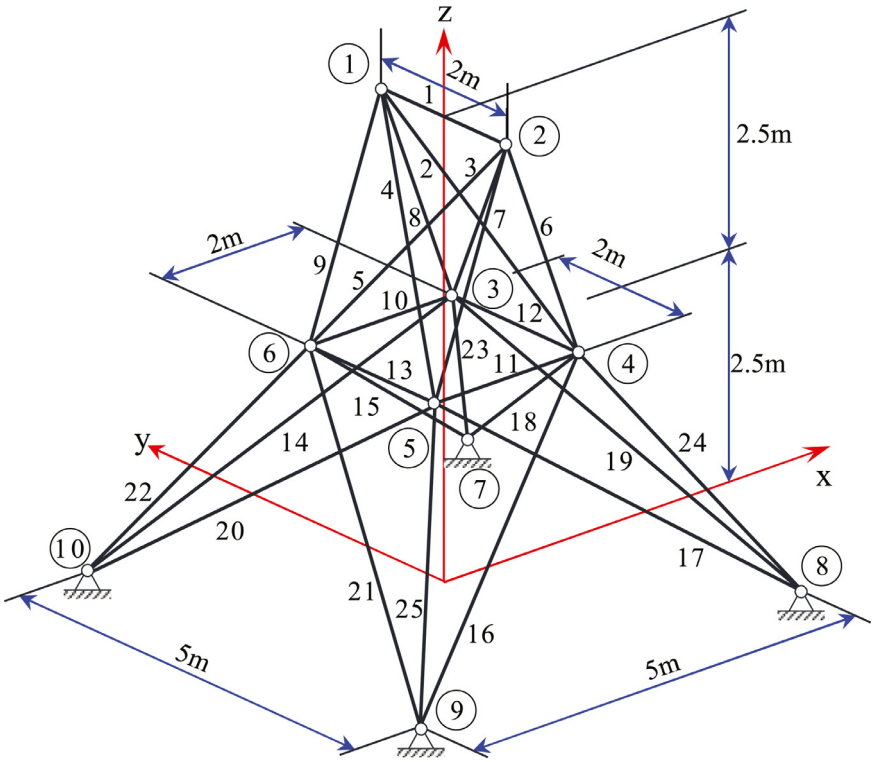

Fig. 13. Schematic of a 25-bar space truss.

Table 13
Comparison of error percentage of different algorithms with FEM for the 25-bar truss.

Error (%)	Case 1			Case 2			Case 3		
	HS	PSO	Present	HS	PSO	Present	HS	PSO	Present
				Displacements					
Min	0.0403	0.0488	0.0002	0.0108	0.0039	0.0004	0.0060	0.0033	0.0001
Max	6.5744	2.5229	0.0257	1.3598	3.1064	0.2142	1.2358	2.3119	0.0921
Mean	1.2672	0.8013	0.0093	0.3311	0.5678	0.0490	0.2210	0.3745	0.0167
				Member forces					
Min	0.0215	0.0000	0.0000	0.0136	0.0209	0.0027	0.0008	0.0084	0.0020
Max	3.5254	2.9808	0.1201	1.3169	0.9953	0.0725	4.7298	5.3105	0.4561
Mean	0.5981	0.5942	0.0244	0.2755	0.3451	0.0270	0.4321	0.5405	0.0353

Table 14
Comparison of deflection results for the 52-bar dome truss obtained by different algorithms.

Disp no. (mm)	Mai et al. [26]	FEM	Present	Error (%)
w_1	1.328	1.3276	1.3218	0.436
w_2	0.720	0.7202	0.7251	0.677
w_6	10.000	10.0089	10.0199	0.109
w_7	10.000	10.0078	9.9813	0.265
Π_p(kN.cm)	–	−599.3685	−599.3687	0.000

4.2.2. 52-bar dome truss

A 52-bar dome truss shown in Fig. 14 is investigated for the next geometrical nonlinear analysis. The optimal cross-sectional area of members obtained by Mai et al. [26] is used to perform this analysis, and they are classified into 8 groups, where $A_1 = A_2 = A_3 = A_4 = A_8 = 2$ cm^2, $A_5 = 16.672$ cm^2, $A_6 = 17.585$ cm^2, and $A_7 = 2.519$ cm^2. All members are made of a linearly elastic material MAT6 with Young's modulus E = 21000 kN/cm^2. The system is subjected to a downward concentrated load $P_z = 150$ kN at joints 6–13. The network configuration for training is mentioned in Table 1.

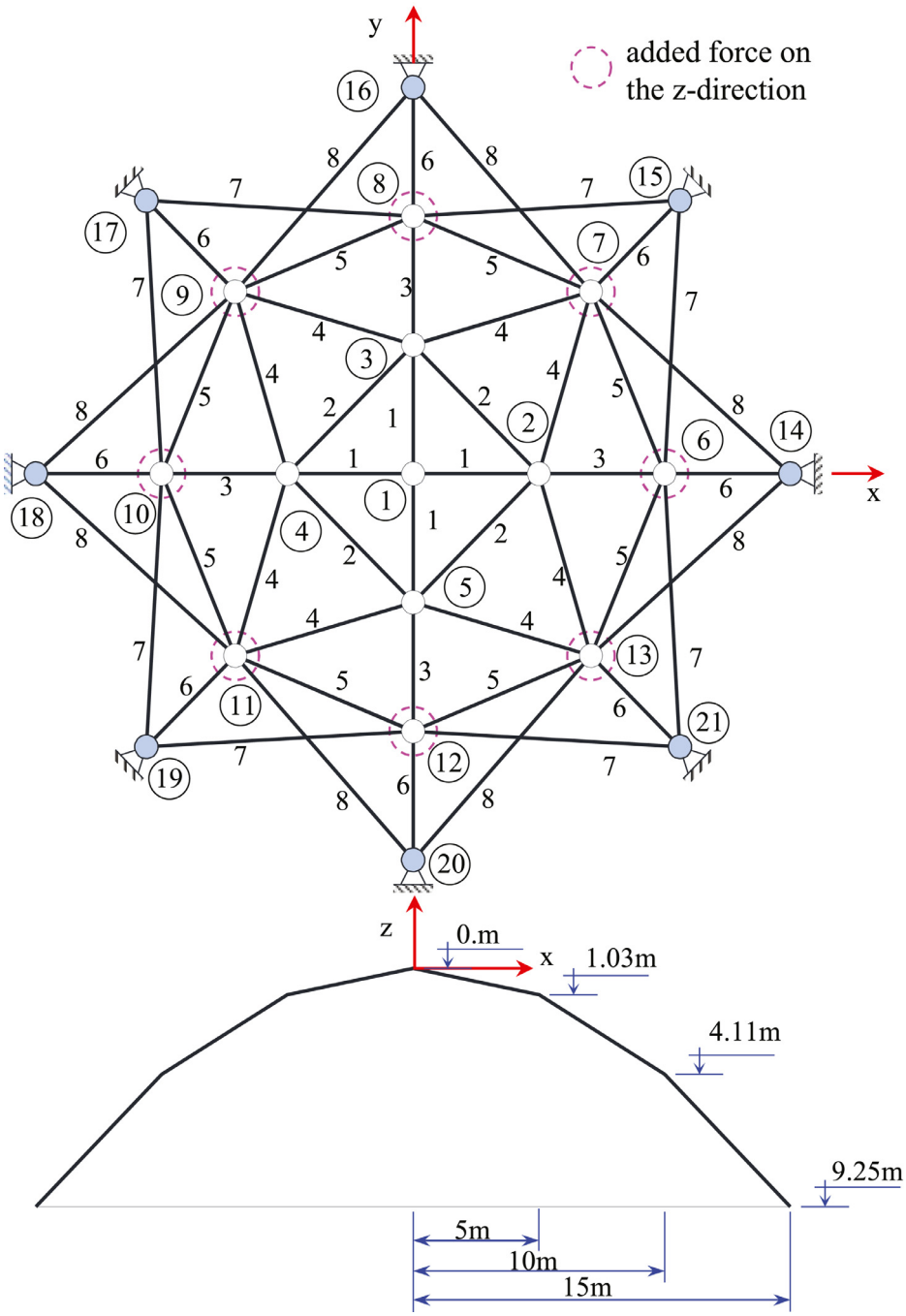

Fig. 14. 52-bar dome space truss structure.

As the previously indicated problems, Tables 14 and 15 summarize the analysis results achieved by the present study and other methods. Firstly, it can be observed that the minimum energy (−599.3687 kN.cm) acquired by NN is smaller than FEM (−599.3685 kN.cm). Otherwise, the differences of (0.109–0.677)% for displacement and (0.052–1.430)% for member force are observed compared with FEM. Although the maximum relative error of the member force is 1.43%, it should be noted that the accuracy of the FEM solution depends on the choice of control parameters used in the nonlinear solution technique [26]. Fig. 15 shows the potential energy convergence history obtained by NN. It indicates that the network rapidly converges in the first 200 epochs, and approaches the optimal solution after 400 epochs.

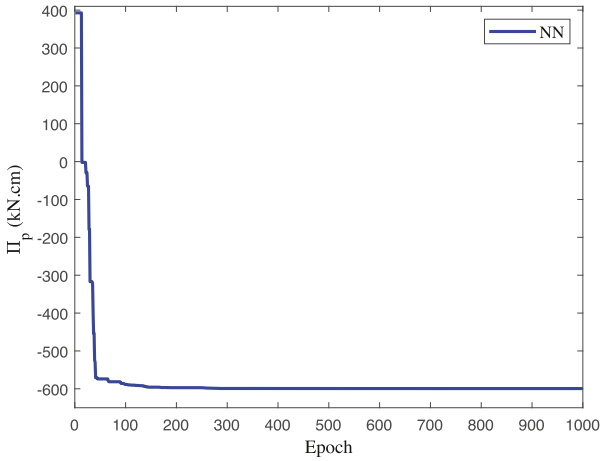

Fig. 15. The convergence history of the loss function for the 52-bar dome truss.

Table 15
Comparison of member forces for 52-bars truss obtained by different algorithms.

Force (N)	Connection	FEM	Present	Error (%)
f_1	1–2	0.0000	0.0000	0.790
f_5	2–3	1.0506	1.0391	1.095
f_9	2–6	2.9809	2.9383	1.430
f_{12}	2–7	2.9809	2.9383	1.430
f_{21}	6–7	−174.8488	−174.7141	0.077
f_{29}	6–14	−185.2631	−185.1668	0.052
f_{30}	7–15	−194.1764	−193.9626	0.110
f_{37}	6–15	−18.3382	−18.3529	0.080
f_{45}	7–14	−14.6041	−14.5690	0.241

Table 16
Comparison of member forces for the 10-bar truss with different algorithms and various materials.

Forces ($\times 10^3$ kg)	MATA			MATB			MATC		
	ILM [18]	CEMP [18]	Present	ILM [18]	CEMP [18]	Present	ILM [18]	CEMP [18]	Present
f_1	−299.800	−299.600	−299.7776	−299.900	−300.300	−299.9140	−299.700	−299.700	−299.7381
f_2	−110.400	−111.300	−110.3785	−104.800	−104.500	−104.8231	−106.900	−107.300	−106.8638
f_3	−141.700	−142.000	−141.7359	−141.500	−140.900	−141.5430	−141.800	−141.900	−141.7916
f_4	141.100	140.900	141.1068	141.300	141.900	141.2998	141.100	141.000	141.0511
f_5	−10.200	−11.900	−10.1559	−4.700	−4.900	−4.7371	−6.600	−7.000	−6.6020
f_6	−126.700	−124.100	−126.7441	−134.600	−135.000	−134.6006	−131.700	−131.200	−131.7144
f_7	156.100	158.700	156.0986	148.200	147.800	148.2421	151.100	151.700	151.1283
f_8	89.600	87.800	89.6217	95.200	95.500	95.1767	93.100	92.700	93.1363
f_9	300.200	300.400	300.2224	300.100	299.700	300.0860	300.300	300.300	300.2618
f_{10}	89.600	87.800	89.6216	95.200	95.500	95.1769	93.100	92.700	93.1362
Π_p (kg.m)	–	–	−8776.2407	–	–	−9672.8855	–	–	−14544.8473

4.3. Material nonlinearity

In this section, two examples are considered to estimate the efficiency and reliability of the proposed approach for the material nonlinear analysis. Three types of material models, namely MATA, MATB, and MATC, are used here. All members have the same cross-sectional area 100 cm^2. The analysis results obtained are compared with ILM and CEMP [18]. The network architectures, as shown in Table 1, are defined to train the models.

4.3.1. 10-bar planar truss

A 10-bar planar truss is considered to evaluate the material nonlinear behavior. The geometry, loading, and boundary conditions are illustrated in Fig. 16. The final results, including the energy, member forces, and errors, are summarized in Tables 16 and 17. It can be observed that the energy of material MATA (−8776.241 kg.m) is larger than the MATB (−9672.886 kg.m) and MATC (−14544.847 kg.m), so the structure with the material model MATA results in a better deformation than other materials. Clearly, the member forces found by the NN are very close to the results gained by ILM and

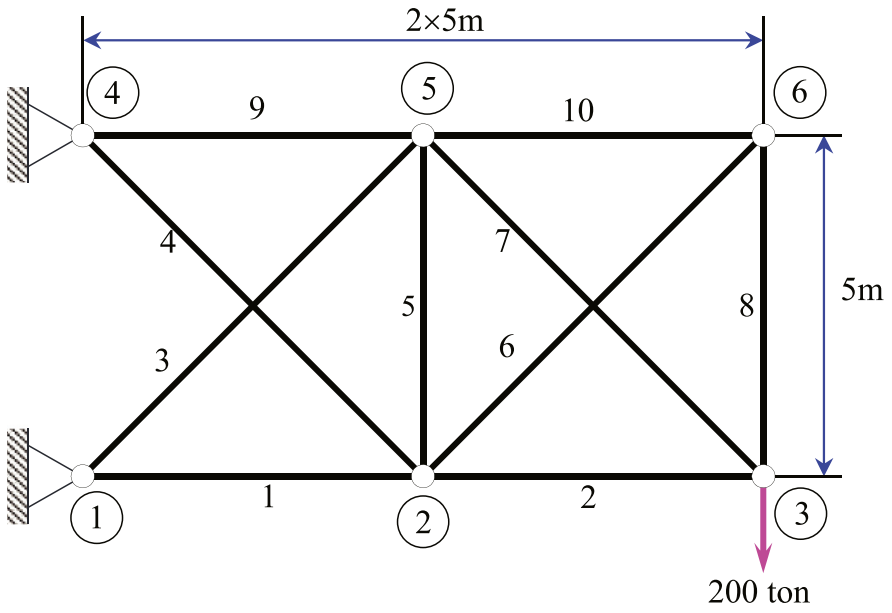

Fig. 16. A 10-bar planar truss structure.

Table 17
Comparison of error percentage of different algorithms with ILM for the 10-bar truss.

Error (%)	MATA		MATB		MATC	
	CEMP	Present	CEMP	Present	CEMP	Present
Min	0.0666	0.0009	0.1333	0.0002	0.0000	0.0059
Max	16.6667	0.4327	4.2553	0.7892	6.0606	0.0390
Mean	2.5704	0.0581	0.6854	0.0929	0.8212	0.0237

Table 18
Comparison of member forces for the 21-bar truss with different algorithms and various materials.

Forces ($\times 10^3$ kg)	MATA			MATB			MATC		
	ILM [18]	CEMP [18]	Present	ILM [18]	CEMP [18]	Present	ILM [18]	CEMP [18]	Present
f_1	171.200	171.300	171.1684	168.600	168.700	168.6476	158.200	158.200	158.1716
f_2	153.400	153.300	153.3964	146.400	146.500	146.4163	123.700	123.700	123.6722
f_6	−242.100	−242.200	−242.0716	−238.500	−238.500	−238.4932	−223.700	−223.700	−223.6901
f_7	303.400	303.300	303.3963	298.700	298.700	298.7314	288.500	288.500	288.4732
f_8	353.200	353.000	353.1582	355.300	355.400	355.3107	357.500	357.600	357.5358
f_9	328.500	328.700	328.5323	330.200	330.100	330.1548	337.300	337.200	337.2644
f_{11}	−204.800	−205.700	−204.7896	−192.200	−192.200	−192.2189	−216.400	−216.400	−216.3917
f_{18}	−214.500	−214.600	−214.5337	−211.200	−211.700	−211.2335	−204.000	−204.000	−203.9817
f_{19}	−203.700	−204.100	−203.7155	−193.200	−193.200	−193.2077	−162.800	−162.700	−162.7884
f_{21}	2.800	2.900	2.8185	3.700	3.800	3.7053	13.200	13.300	13.2244
Π_p (kg.m)	–	–	−26823.3809	–	–	−30395.9725	–	–	−40341.9256

CEMP. According to Ohkubo [17], ILM outperforms the CEMP method when the complementary energy is always lower for each material. Hence, it is used to evaluate the efficiency of the proposed model based on the error percentage. As shown in Table 17, it is easily seen that the maximum relative error of the network is less than 1% while CEMP gained up to 16.6667%, and usually occurs at the 5th element. On the other hand, the mean errors are smaller than 0.1%, and this again shows the effectiveness of the network in the nonlinear analysis.

4.3.2. 21-bar planar truss

The last problem done herein is to analyze a 21-bar planar truss as shown in Fig 17. Tables 18 and 19 show the comparison with the results by CEMP and ILM. As the previous example, the differences in attained results of three methods are almost small and negligible. However, the maximum relative error of our method is less than 0.6603% while CEMP is 3.5714%, and hence the accuracy of the NN is high. Furthermore, the stability is expressed by the average error which is less than 0.1% for three material types.

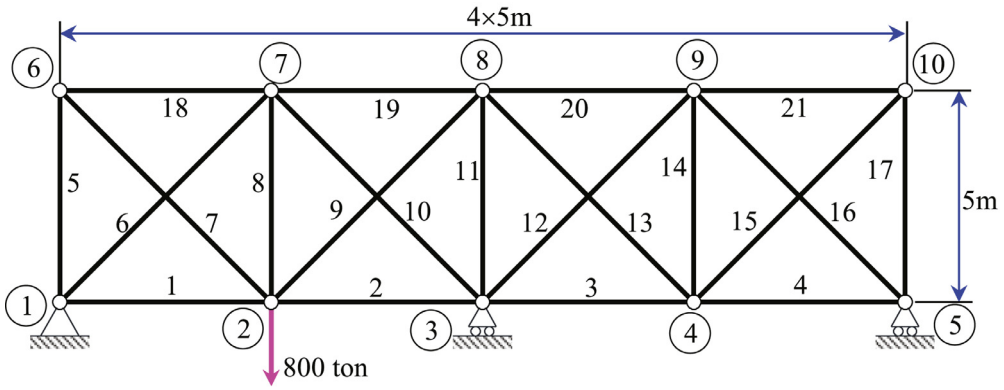

Fig. 17. 21-bar two-span continuous truss structure.

Table 19
Comparison of error percentage of different algorithms with ILM for the 21-bar truss.

Error (%)	MATA		MATB		MATC	
	CEMP	Present	CEMP	Present	CEMP	Present
Min	0.0330	0.0012	0.0000	0.0029	0.0000	0.0038
Max	3.5714	0.6603	2.7027	0.1422	0.7576	0.1846
Mean	0.4569	0.0744	0.3125	0.0241	0.0877	0.0279

5. Conclusions

In this article, an unsupervised NN framework has been successfully developed to solve the geometrically nonlinear analysis of inelastic truss structures. Herein, TPE is constructed as a loss function of the NN model, and it is minimized in the training process. Accordingly, the responses of structures are found at the end of this procedure when achieving the minimum energy. The efficiency and reliability of the proposed method are demonstrated through several numerical examples including geometric nonlinearity, material nonlinearity, and dual nonlinearities. Numerical results pointed out that the nonlinear behavior of truss structures can be simply and accurately solved by the proposed approach without utilizing any incremental-iterative methods in the FEM. One of the interesting things of this paradigm is that its learning possibility is only relied upon the set of the nodal coordinates. Hence, the obtained results are independent of the sampling techniques. Furthermore, there are no complex sensitivity analyses because of employing the automatic differentiation in the paradigm's framework. With those outstanding features, the proposed methodology is promising to provide a new route to handle complex problems in nonlinear structural analysis. However, there have been still an unanswered question about how to determine the optimal architecture network. This will be the next topic of our future investigation.

Declaration of Competing Interest

The authors declare that they have no known competing financial interests or personal relationships that could have appeared to influence the work reported in this paper.

CRediT authorship contribution statement

Hau T. Mai: Conceptualization, Methodology, Software, Formal analysis, Investigation, Writing – original draft, Writing – review & editing, Visualization. **Qui X. Lieu:** Formal analysis, Methodology, Writing – original draft, Writing – review & editing. **Joowon Kang:** Data curation, Validation, Resources. **Jaehong Lee:** Conceptualization, Methodology, Supervision, Funding acquisition.

Acknowledgment

This research was supported by a grant (NRF-2021R1A4A2002855) from NRF (National Research Foundation of Korea) funded by MEST (Ministry of Education and Science Technology) of Korean government.

References

[1] H.-T. Thai, T.-K. Nguyen, S. Lee, V.I. Patel, T.P. Vo, Review of nonlinear analysis and modeling of steel and composite structures, Int. J. Struct. Stab. Dyn. 20 (2020) 2030003.

[2] P. Mata, S. Oller, A. Barbat, Static analysis of beam structures under nonlinear geometric and constitutive behavior, Comput Methods Appl. Mech. Eng. 196 (2007) 4458–4478.
[3] T.P. Vo, J. Lee, Geometrical nonlinear analysis of thin-walled composite beams using finite element method based on first order shear deformation theory, Arch. Appl. Mech. 81 (2011) 419–435.
[4] M. Greco, F. Gesualdo, W. Venturini, H. Coda, Nonlinear positional formulation for space truss analysis, Finite Elem. Anal. Des. 42 (2006) 1079–1086.
[5] C. Taube, H.-G. Timmler, G. Morgenthal, Enhanced method for the nonlinear structural analysis based on direct energy principles, Eng. Struct. 204 (2020) 109789.
[6] R.J. Reilly, E.L. Sutton, An iterative solution for geometrically nonlinear trusses, Comput. Struct. 3 (1973) 1053–1061.
[7] A.K. Noor, J.M. Peters, Nonlinear dynamic analysis of space trusses, Comput. Methods Appl. Mech. Eng. 21 (1980) 131–151.
[8] Y. Peng, Z. Li, M.M. Kamel, Geometrical nonlinear problems of truss beam by base force element method, Int. J. Numer. Methods Eng. 122 (2021) 4793–4824.
[9] M. Crisfield, J.L. Tassoulas, Non-linear finite element analysis of solids and structures, volume 1, J. Eng. Mech. 119 (1993) 1504–1505.
[10] J.N. Reddy, An Introduction to Nonlinear Finite Element Analysis, With Applications to Heat Transfer, Fluid Mechanics, and Solid Mechanics, second ed., OUP Oxford, 2014.
[11] A. Maghami, F. Shahabian, S.M. Hosseini, Path following techniques for geometrically nonlinear structures based on multi-point methods, Comput. Struct. 208 (2018) 130–142.
[12] A. Maghami, F. Shahabian, S.M. Hosseini, Geometrically nonlinear analysis of structures using various higher order solution methods: a comparative analysis for large deformation, Comput. Model. Eng. Sci. 121 (2019) 877–907.
[13] R. Fox, E. Stanton, Developments in structural analysis by direct energy minimization, AIAA J. 6 (1968) 1036–1042.
[14] A. Kaveh, H. Rahami, Nonlinear analysis and optimal design of structures via force method and genetic algorithm, Comput. Struct. 84 (2006) 770–778.
[15] Y.C. Toklu, G. Bekdaş, R. Temur, Analysis of trusses by total potential optimization method coupled with harmony search, Struct. Eng. Mech. 45 (2013) 183–199.
[16] R. Temür, Y.S. Türkan, Y.C. Toklu, Geometrically nonlinear analysis of trusses using particle swarm optimization, in: Recent Advances in Swarm Intelligence and Evolutionary Computation, Springer, 2015, pp. 283–300.
[17] S. Ohkubo, Y. Watada, F. Toshio, Nonlinear analysis of truss by energy minimization, Comput. Struct. 27 (1987) 129–145.
[18] Y. Toklu, Nonlinear analysis of trusses through energy minimization, Comput. Struct. 82 (2004) 1581–1589.
[19] J. Bohn, M. Feischl, Recurrent neural networks as optimal mesh refinement strategies, Comput. Math. Appl. 97 (2021) 61–76.
[20] S. Zhu, M. Ohsaki, X. Guo, Prediction of non-linear buckling load of imperfect reticulated shell using modified consistent imperfection and machine learning, Eng. Struct. 226 (2021) 111374.
[21] Q.X. Lieu, K.T. Nguyen, K.D. Dang, S. Lee, J. Kang, J. Lee, An adaptive surrogate model to structural reliability analysis using deep neural network, Expert Syst. Appl. 189 (2022) 116104.
[22] S. Srinivasan, M.Z. Saghir, Modeling of thermotransport phenomenon in metal alloys using artificial neural networks, Appl. Math. Model. 37 (2013) 2850–2869.
[23] T.T. Truong, S. Lee, J. Lee, An artificial neural network-differential evolution approach for optimization of bidirectional functionally graded beams, Compos. Struct. 233 (2020) 111517.
[24] O. San, R. Maulik, Machine learning closures for model order reduction of thermal fluids, Appl. Math. Model. 60 (2018) 681–710.
[25] H. Wessels, C. Weißenfels, P. Wriggers, The neural particle method–an updated lagrangian physics informed neural network for computational fluid dynamics, Comput. Methods Appl. Mech. Eng. 368 (2020) 113127.
[26] H.T. Mai, J. Kang, J. Lee, A machine learning-based surrogate model for optimization of truss structures with geometrically nonlinear behavior, Finite Elem. Anal. Des. 196 (2021) 103572.
[27] H.T. Mai, Q.X. Lieu, J. Kang, J. Lee, A novel deep unsupervised learning-based framework for optimization of truss structures, Eng. Comput. (2022).
[28] A. Chandrasekhar, K. Suresh, Tounn: topology optimization using neural networks, Struct. Multidiscip. Optim. 63 (2021) 1135–1149.
[29] D.A. White, W.J. Arrighi, J. Kudo, S.E. Watts, Multiscale topology optimization using neural network surrogate models, Comput. Methods Appl. Mech. Eng. 346 (2019) 1118–1135.
[30] T.T. Truong, D. Dinh-Cong, J. Lee, T. Nguyen-Thoi, An effective deep feedforward neural networks (DFNN) method for damage identification of truss structures using noisy incomplete modal data, J. Build. Eng. 30 (2020) 101244.
[31] S. Lee, S. Park, T. Kim, Q.X. Lieu, J. Lee, Damage quantification in truss structures by limited sensor-based surrogate model, Appl. Acoust. 172 (2021) 107547.
[32] H. Tran-Ngoc, S. Khatir, H. Ho-Khac, G. De Roeck, T. Bui-Tien, M.A. Wahab, Efficient artificial neural networks based on a hybrid metaheuristic optimization algorithm for damage detection in laminated composite structures, Compos. Struct. 262 (2021) 113339.
[33] H. Tran-Ngoc, S. Khatir, T. Le-Xuan, G. De Roeck, T. Bui-Tien, M.A. Wahab, A novel machine-learning based on the global search techniques using vectorized data for damage detection in structures, Int. J. Eng. Sci. 157 (2020) 103376.
[34] S. Khatir, S. Tiachacht, C.L. Thanh, E. Ghandourah, S. Mirjalili, M.A. Wahab, An improved artificial neural network using arithmetic optimization algorithm for damage assessment in FGM composite plates, Compos. Struct. 273 (2021) 114287.
[35] D.H. Nguyen-Le, Q. Tao, V.-H. Nguyen, M. Abdel-Wahab, H. Nguyen-Xuan, A data-driven approach based on long short-term memory and hidden Markov model for crack propagation prediction, Eng. Fract. Mech. 235 (2020) 107085.
[36] S. Khatir, D. Boutchicha, C.L. Thanh, H. Tran-Ngoc, T. Nguyen, M. Abdel-Wahab, Improved ANN technique combined with Jaya algorithm for crack identification in plates using XIGA and experimental analysis, Theor. Appl. Fract. Mech. 107 (2020) 102554.
[37] W. Li, M.Z. Bazant, J. Zhu, A physics-guided neural network framework for elastic plates: comparison of governing equations-based and energy-based approaches, Comput. Methods Appl. Mech. Eng. 383 (2021) 113933.
[38] P. Hajela, L. Berke, Neurobiological computational models in structural analysis and design, Comput. Struct. 41 (1991) 657–667.
[39] L. Berke, P. Hajela, Applications of artificial neural nets in structural mechanics, in: Shape and Layout Optimization of Structural Systems and Optimality Criteria Methods, Springer, 1992, pp. 331–348.
[40] S. Lee, J. Ha, M. Zokhirova, H. Moon, J. Lee, Background information of deep learning for structural engineering, Arch. Comput. Methods Eng. 25 (2018) 121–129.
[41] L. Liang, M. Liu, C. Martin, W. Sun, A deep learning approach to estimate stress distribution: a fast and accurate surrogate of finite-element analysis, J. R. Soc. Interface 15 (2018) 20170844.
[42] J. Alam, Application of Artificial Neural Networks in Nonlinear Analysis of Trusses, vol. 105319, Lewis Research Center, 1991.
[43] A. Maghami, S.M. Hosseini, Intelligent step-length adjustment for adaptive path-following in nonlinear structural mechanics based on group method of data handling neural network, Mech. Adv. Mater. Struct. 28 (2021) 1–28.
[44] N. Feng, G. Zhang, K. Khandelwal, Finite strain FE2 analysis with data-driven homogenization using deep neural networks, Comput. Struct. 263 (2022) 106742.
[45] H.J. Logarzo, G. Capuano, J.J. Rimoli, Smart constitutive laws: inelastic homogenization through machine learning, Comput Methods Appl. Mech. Eng. 373 (2021) 113482.
[46] L. Wu, N.G. Kilingar, L. Noels, et al., A recurrent neural network-accelerated multi-scale model for elasto-plastic heterogeneous materials subjected to random cyclic and non-proportional loading paths, Comput. Methods Appl. Mech. Eng. 369 (2020) 113234.
[47] F. Ghavamian, A. Simone, Accelerating multiscale finite element simulations of history-dependent materials using a recurrent neural network, Comput. Methods Appl. Mech. Eng. 357 (2019) 112594.

[48] E. Haghighat, M. Raissi, A. Moure, H. Gomez, R. Juanes, A physics-informed deep learning framework for inversion and surrogate modeling in solid mechanics, Comput. Methods Appl. Mech. Eng. 379 (2021) 113741.
[49] V.M. Nguyen-Thanh, X. Zhuang, T. Rabczuk, A deep energy method for finite deformation hyperelasticity, Eur. J. Mech. - A/Solids 80 (2020) 103874.
[50] D.W. Abueidda, Q. Lu, S. Koric, Meshless physics-informed deep learning method for three-dimensional solid mechanics, arXiv:2012.01547(2020).
[51] H. Guo, X. Zhuang, T. Rabczuk, A deep collocation method for the bending analysis of Kirchhoff plate, arXiv:2102.02617(2021).
[52] X. Zhuang, H. Guo, N. Alajlan, H. Zhu, T. Rabczuk, Deep autoencoder based energy method for the bending, vibration, and buckling analysis of Kirchhoff plates with transfer learning, Eur. J. Mech. - A/Solids 87 (2021) 104225.
[53] N. Zobeiry, K.D. Humfeld, A physics-informed machine learning approach for solving heat transfer equation in advanced manufacturing and engineering applications, Eng. Appl. Artif. Intell. 101 (2021) 104232.
[54] E. Haghighat, A.C. Bekar, E. Madenci, R. Juanes, A nonlocal physics-informed deep learning framework using the peridynamic differential operator, Comput. Methods Appl. Mech. Eng. 385 (2021) 114012.
[55] J.N. Reddy, Introduction to the Finite Element Method, McGraw-Hill Education, 2019.
[56] M.A. Crisfield, Nonlinear Finite Element Analysis of Solids and Structures. Volume 1: Essentials, 1991.
[57] W. Jenkins, A neural network for structural re-analysis, Comput. Struct. 72 (1999) 687–698.
[58] H.-T. Kang, C.J. Yoon, Neural network approaches to aid simple truss design problems, Comput. - Aided Civ. Infrastruct. Eng. 9 (1994) 211–218.
[59] M. Paul, Applied machine learning, 2018, (https://cmci.colorado.edu/classes/INFO-4604/resources.html). Accessed: 2021-04-19.
[60] D.P. Kingma, J. Ba, Adam: a method for stochastic optimization, arXiv:1412.6980(2014).